

# Unexpected results for the non-trivial fusion of Majorana zero modes in interacting quantum-dot arrays

Bradraj Pandey,<sup>1,2</sup> Satoshi Okamoto,<sup>2</sup> and Elbio Dagotto<sup>1,2</sup>

<sup>1</sup>*Department of Physics and Astronomy, The University of Tennessee, Knoxville, Tennessee 37996, USA*

<sup>2</sup>*Materials Science and Technology Division, Oak Ridge National Laboratory, Oak Ridge, Tennessee 37831, USA*

(Dated: December 14, 2023)

Motivated by recent experimental reports of Majorana zero modes (MZMs) in quantum-dot systems at the “sweet spot”, where the electronic hopping  $t_h$  is equal to the superconducting coupling  $\Delta$ , we study the time-dependent spectroscopy corresponding to the *non-trivial* fusion of MZMs. The expression non-trivial refers to the fusion of Majoranas from different original pairs of MZMs, each with well-defined parities. For the first time, we employ an experimentally accessible time-dependent real-space local density-of-states (LDOS) method to investigate the non-trivial MZMs fusion outcomes in canonical chains and in a Y-shape array of interacting electrons. In the case of quantum-dot chains where two pairs of MZMs are initially disconnected, after fusion we find equal-height peaks in the electron and hole components of the LDOS, signaling non-trivial fusion into both the vacuum  $I$  and fermion  $\Psi$  channels with equal weight. For  $\pi$ -junction quantum-dot chains, where the superconducting phase has opposite signs on the left and right portions of the chain, after the non-trivial fusion, surprisingly we observed the formation of an exotic two-site MZM near the center of the chain, coexisting with another single-site MZM. Furthermore, we also studied the fusion of three MZMs in the Y-shape geometry. In this case, after the fusion we observed the novel formation of another exotic multi-site MZM, with properties depending on the connection and geometry of the central region of the Y-shape quantum-dot array.

## Introduction

Majorana zero modes are attracting much attention due to their potential application in developing fault-tolerant quantum computation [1–3]. The Majorana zero modes (MZMs) follow non-Abelian statistics and allow the non-local encoding of quantum information, which makes MZMs good candidates to utilize as qubits in topological quantum computations [3–5]. Recently, in coupled quantum-dot systems, a pair of localized MZMs were observed in the tunneling conductance measurements at the sweet spot  $t_h = \Delta$ , where the electronic hopping  $t_h$  and superconducting coupling  $\Delta$  are equal in magnitude [6]. These quantum-dot systems [7–11] allow to realize the idealized Kitaev chain with gate-tunable experimental parameters [12–14]. Realizing MZMs via quantum dots significantly reduces the problem of formation and detection of the MZMs, as compared to the more standard proximitized semiconducting nano-wire systems which are affected by random disorder [7, 15].

This recent experimental progress in quantum-dot systems provides a platform to test the non-Abelian statistics of Majorana fermionic candidates [6]. Fusion and braiding are two fundamental characteristics of non-Abelian anyons [16, 17]. The realization of MZMs at the sweet spot allows the study of the fusion and braiding of MZMs even in small systems [6] (because in this case the MZMs are fully localized at a single site), as compared to the semiconducting nanowires that need a more extensive system. The sweet spot also facilitates analytical calculations for special cases [18, 19]. The fusion of MZMs and detection of their outcomes in quantum-dot experiments are expected to be easier than performing braiding of MZMs in other platforms.

The multiple fusion outcomes of MZMs,  $\gamma \times \gamma = I + \Psi$ , are related to their non-Abelian statistics [3], because two MZMs

( $\gamma$ ) after fusion can result in either vacuum ( $I$ ) or a fermion ( $\Psi$ ) [16]. However, the fusion of MZMs can be designed in two ways, namely a “trivial” and a “non-trivial” procedure. In the trivial case, the fusion outcome is deterministic (either a full electron or full hole) as the fusion of MZMs occurs within the same pair with well-defined parity +1 or -1. This trivial fusion can be performed using just one pair of MZMs in a chain, by moving one edge MZM towards the other edge MZM [20]. On the other hand, the non-trivial fusion refers to the fusion of Majoranas belonging to different initially disconnected pairs of MZMs each with pre-defined parities. In this non-trivial case, the fusion outcomes becomes probabilistic [16], not deterministic, and can yield both electron and hole. In order to perform non-trivial MZMs, we need at least two-pairs of MZMs, i.e. at least four MZMs. This paper mainly focuses on the time-dependent non-trivial fusion using two and three pairs of MZMs in models simulating interacting quantum-dot systems.

For the more canonical semiconductor nanowire setups, the detection of the fusion outcome of MZMs has been proposed by charge sensing based on dynamical Bogoliubov-de Gennes simulations [16, 21, 22]. Recently, in the context of coupled quantum dots, the detection of the fusion of MZMs has been suggested using the parity readout of the systems [23]. Even without fusing the MZMs, by preparing the two pairs of MZMs in two different ways, the testing of fusion outcome has been proposed by observing the fermionic parity readout (deterministic or probabilistic) [23]. Compared to previous theoretical studies, here we propose for the first time detecting fusion outcomes using a time-dependent real-space local density-of-states method (LDOS( $\omega, t$ )) [20] in both canonical chains and in Y-shape arrays of interacting quantum dots. The LDOS( $\omega, t$ ) should be experimentally accessible via tunneling conductance measurements in the

existing quantum-dot setups [6, 24].

(a) One dimensional chain



(b) Y-shape geometry

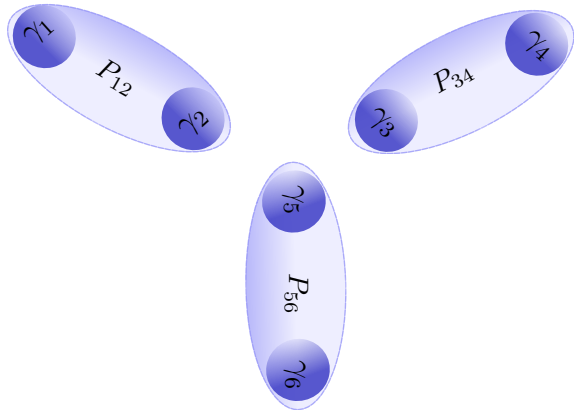


FIG. 1. Non-trivial fusion of Majoranas. (a) Schematic representation of two pairs of Majorana zero modes ( $[\gamma_1, \gamma_2]$  and  $[\gamma_3, \gamma_4]$ ) in a quantum dot array. At time  $t = 0$ , the parities of the left  $P_{12} = -i\langle\gamma_1\gamma_2\rangle$  and right  $P_{34} = -i\langle\gamma_3\gamma_4\rangle$  pairs of MZMs are well defined. There is no hopping and no pairing coupling between the Majoranas  $\gamma_2$  and  $\gamma_3$ . (b) Schematic representation of the three-pairs of Majoranas zero modes in Y-shape geometry. At time  $t = 0$ , the parities of three pairs of MZMs  $P_{12} = -i\langle\gamma_1\gamma_2\rangle$ ,  $P_{34} = -i\langle\gamma_3\gamma_4\rangle$  and  $P_{56} = -i\langle\gamma_5\gamma_6\rangle$  are well defined. Initially, there is no hopping and pairing coupling between the three central Majoranas  $\gamma_2, \gamma_3$  and  $\gamma_5$ . For non-trivial fusion, the time-dependent hopping and pairing amplitude between the different pairs of MZMs were varied with time.

Motivated by the recent experimental realization of a minimal Kitaev chain in quantum dots coupled by a short superconductor-semiconductor hybrid (SC-SM) [6, 25], here we study the non-trivial fusion of MZMs in quantum-dot arrays at the sweet spot ( $t_h = \Delta$ ). In the quantum dot experiments, the hopping and superconducting coupling between the quantum dots are tunable by changing the electrostatic gate [12, 14, 26]. In this work, to observe the time-dependent non-trivial fusion, we tune the time-dependent hopping and superconducting coupling between quantum-dot arrays, where two different pairs of MZMs exist with pre-defined parities. We implement the time-dependent exact-diagonalization method using all the many-body states of interacting electrons of finite-size systems to study the spectroscopy of the non-trivial fusion of MZMs [20]. In the case of two one-dimensional chains with two pairs of MZMs (see Fig. 1a), we find equal height peaks in the electron and hole components of the LDOS( $\omega, t$ ), showing

the formation of both electron  $\Psi$  and vacuum channels. Surprisingly, due to the non-equilibrium effects and parity conservation of the time-evolving many-body state, we find the equal magnitude of electron and hole peaks at both  $\pm\omega$  energies in LDOS( $\omega, t$ ). In contrast to previous studies, for the first time we discuss the effect of repulsive Coulomb interaction on non-trivial fusion. We find an asymmetry in the LDOS( $\omega, t$ ) peaks at  $\pm\omega$  with increase in repulsive Coulomb interaction.

For the  $\pi$ -junction, where the two pairs of MZMs are initialized with opposite signs of the pairing amplitude after the fusion, we find that one of the central MZMs remains unaffected, while the second single-site MZM is transformed to a two-site non-local MZM. In fact, we find that this two-site MZM is formed after *tunneling* through the centrally localized one-site MZM. The tunneling of *half* of the second MZM through another centrally localized one-site MZM is a novel effect in a strictly one-dimensional geometry [27].

Furthermore, we study the time-dependent fusion of an odd number (three) of Majoranas, where the three pairs of MZMs are initialized in a Y-shape geometry (see Fig. 1b). Surprisingly, during the fusion process we find zero energy peaks in the LDOS( $\omega, t$ ) for three different central sites in addition to the electron and hole peaks at finite energies. After the fusion of Majoranas, we find the formation of an exotic multi-site MZM. Interestingly, the nature of multi-site MZMs depends on the connection and direction of the couplings near the center, which joins the legs of a Y-shape quantum-dot array.

## Results

### Non-trivial fusion of MZMs in one-dimensional chain

In this section, we will consider two one-dimensional quantum-dot arrays at the sweet-spot, with the same sign for the superconducting phase ( $\phi_1 = \phi_2 = 0$ ). These two left and right short wires are coupled through time-dependent hopping ( $t_h(t)$ ) and pairing ( $\Delta(t)$ ) terms, which can be tuned by changing the gate potential adiabatically. In the quantum-dot experiment the hopping and pairing terms between the two quantum dots are tuned by modifying the properties of Andreev bound states in a superconductor-semiconductor hybrid (SC-SM) [14, 26]. These properties are controlled by an electrostatic gate connected to the SC-SM hybrid segment. The effective Hamiltonian for the quantum-dots arrays under the approximation of using only one level per quantum dot then becomes:

$$H^L = \sum_{j=1}^{l-1} \left( -t_h c_j^\dagger c_{j+1} + e^{i\phi_1} \Delta c_j c_{j+1} + H.c. \right), \quad (1)$$

$$H^R = \sum_{j=l+1}^{2l} \left( -t_h c_j^\dagger c_{j+1} + e^{i\phi_2} \Delta c_j c_{j+1} + H.c. \right), \quad (2)$$

$$H^C(t) = \left( -t_h(t) c_l^\dagger c_{l+1} + \Delta(t) c_l c_{l+1} + H.c. \right). \quad (3)$$

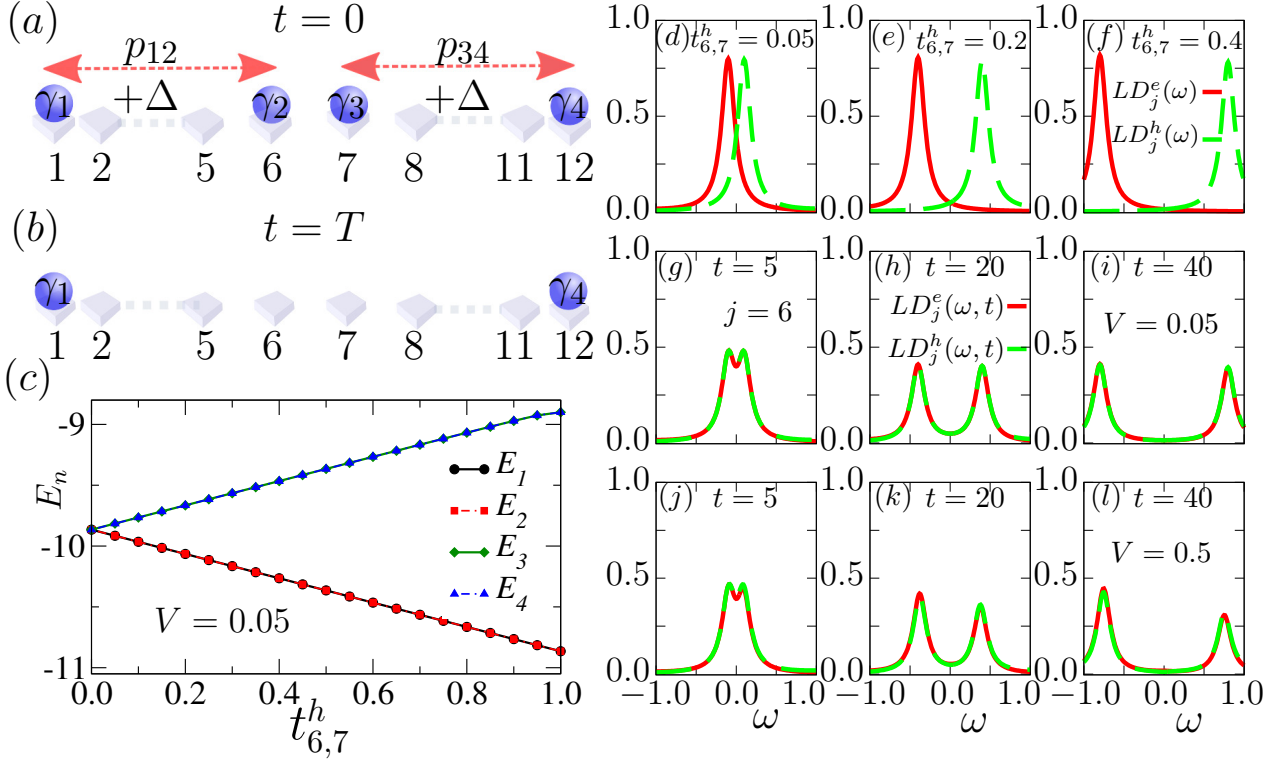


FIG. 2. (a) Schematic representation of two pairs of MZMs using a 12-sites quantum dots array with same left and right superconducting phases  $\phi_1 = \phi_2 = 0$ . At time  $t = 0$ , there is no hopping and no pairing coupling between the Majoranas  $\gamma_2$  and  $\gamma_3$ . The time-dependent hopping and pairing coupling between sites  $j = 6$  and  $7$  can be established by reducing the “barrier” between the left and right portions of the 12-site chain, leading to the non-trivial fusion of the central MZMs  $\gamma_2$  and  $\gamma_3$ . (b) After the fusion at time  $t = T$ , the system has one MZM at each end site. (c) Four lowest many-body-eigenstates  $E_n$  vs. the linear variation in hopping  $t_{6,7}^h$  and pairing terms of the central bond. Each line shown has degeneracy two. (d,e,f) The ground state electron and hole portions of the  $LD(\omega, j)$  varying the parameters  $t_{6,7}^h$  and  $\Delta_{6,7}$  at site  $j = 6$  and for the cases  $t_{6,7}^h = 0.05, 0.2$  and  $0.4$ . (g,h,i) The electron and hole components of the time-dependent  $LD(\omega, t, j)$  at site  $j = 6$  and for different times  $t$ , at  $V = 0.05$ . (j,k,l) The  $LD^e(\omega, t, j)$  and  $LD^h(\omega, t, j)$  at site  $j = 6$  at different times  $t$  and for  $V = 0.5$ .

The Coulomb interaction between quantum dots is the standard:

$$H^{Int} = \sum_{j=1}^{2l} (V n_j n_{j+1}). \quad (4)$$

### (a) The case $\phi_1 = \phi_2 = 0$

At time  $t = 0$ , there is no hopping and superconducting coupling between the two wires. As shown in Fig. 2a, the system has two separate pairs of MZMs  $(\gamma_1, \gamma_2)$  and  $(\gamma_3, \gamma_4)$ , with well defined parities  $P_{12} = -i\langle \gamma_1 \gamma_2 \rangle = -1$  and  $P_{34} = -i\langle \gamma_3 \gamma_4 \rangle = -1$ . The total parity (full system) of the initial many-body state can be calculated as  $P_{tot} = e^{i\pi \sum_j n_j}$  [28]. The presence of four MZMs at  $t = 0$  results in a four-fold degenerate ground state, as we can potentially create two spinless fermions by combining these four MZMs in pairs (thus we have degeneracy  $2^2 = 4$ ). Fusing the MZMs within the same pair (with parity  $-1$  as example), namely  $\gamma_1$  and  $\gamma_2$  or  $\gamma_3$  and  $\gamma_4$ , using a height-variable potential wall in between them, results in the formation of a full electron (trivial fusion) [20]. This trivial fusion reveals only one fusion channel  $\Psi$  with deterministic formation of a full electron. On

the other hand, the non-trivial fusion of our focus in this paper is expected to produce both fusion channels and a more exotic intermediate dynamics.

We first start with the static case, i.e by varying the hopping ( $t_{6,7}^h$ ) and pairing ( $\Delta_{6,7}$ ) terms between two wire segments linearly as a parameter. The coupling term between the left and right portions of the arrays, using the transformation  $c_j = \frac{1}{\sqrt{2}} (\gamma_j^A + i\gamma_j^B)$  at  $t_{6,7}^h = \Delta_{6,7}$ , can be written in terms of Majorana operators as  $H_{6,7}^C = 2i\Delta_{6,7}\gamma_6^B\gamma_7^A$ . By changing  $\Delta_{6,7}$  the two central Majoranas will overlap, leading to the breaking of the four-fold degeneracy of the ground state. The four-fold degenerate ground state splits into two pairs  $[(E_1, E_2)$  and  $(E_3, E_4)]$  of two-fold degenerate states with combination of even and odd fermion parity (see Fig. 2c). In order to observe the fusion outcome, we calculate the electron  $LD_j^e(\omega)$  and hole  $LD_j^h(\omega)$  components of the local-density-of-states at site  $j = 6$  (site  $j = 7$  has similar  $LD_j(\omega)$  by symmetry).

Using the eigenvectors  $\{|\Psi_m\rangle\}$  of the Hamiltonian  $H$  (Eqs. 1-4), the electronic component of the local density-of-states ( $LD_j(\omega)$ ) for site  $j$  can be written as [20,

29]:

$$LD_j^e(\omega, ) = -\frac{1}{\pi} Im \left( \sum_m \frac{|\langle \Psi_m | c_j | \Psi_1 \rangle|^2}{\omega + E_m - E_1 + i\eta} \right). \quad (5)$$

At  $\Delta_{6,7} = t_{6,7}^h = 0$ , the peak at  $\omega = E_1 - E_m = 0$  in  $LD_j^e(\omega)$  for site  $j = 6$  arises from the transition between degenerate ground states ( $m = 2$  and  $m = 1$ ) with opposite fermionic parity. The hole part  $LD_j^h(\omega)$  also shows an equal height peak at  $\omega = 0$ , indicating the presence of a localized MZM at site  $j = 6$  (and at  $j = 7$ ). By changing  $t_{6,7}^h$ , as shown in Fig. 2(d,e,f), the electron part  $LD_j^e(\omega)$  shows peaks close to  $\omega = -2t_{6,7}^h$ , whereas the hole part shows peaks close to  $\omega = +2t_{6,7}^h$ , displaying the formation of both an electron and a hole at finite  $\omega$ . These electron and hole components of  $LD_j(\omega)$  have equal height, within numerical accuracy, for smaller values of  $V = 0.05$ , confirming the formation of equal magnitude electron and hole components during the non-trivial fusion of two central Majoranas.

However, in real experiments of fusion of MZMs, one needs to change the hopping and pairing amplitude as a function of time close to the adiabatic limit in a dynamical way, as opposed to simply modifying parameters in the Hamiltonian and re-diagonalizing at each time. Namely, in the real experiments the outcome depends on the initial condition and on the speed of the process.

Here, we perform time-dependent fusion of MZMs by changing the hopping according to the formula  $t_h(t) = t_h(T) \frac{n\delta t}{\tau}$ , where  $1/\tau$  is the quenched rate,  $\delta t = 0.001$  is the small time step we used, and  $n$  is the integer number of those steps, such that the  $t_h(t)$  at sites  $j = 6$  and  $7$  increases approximately linearly from 0 to 1 in a time  $\tau = 100$ . At final time  $t = T$ , the time dependent hopping becomes equal to  $t_h(T) = 1$ . For the time evolution, we chose the initial many-body state  $|\Psi(0)\rangle$  with total parity  $P_{tot} = +1$  (this parity is chosen because it corresponds to the ground state at nonzero  $V$ ).

To observe the fusion outcomes at intermediate time  $t$ , first we evolve the initial many-body state  $|\Psi(0)\rangle$  up to time  $t$ , then we calculate the time-dependent electron  $LD_j^e(\omega, t)$  and hole  $LD_j^h(\omega, t)$  parts of the local-density of states (see Method section). Using the eigenvectors of the instantaneous Hamiltonian  $H_I(t)$  and  $|\Psi(t)\rangle$  at time  $t$ , the electronic component of  $LD_j(\omega, t)$  at site  $j$  can be written as  $LD_j^e(\omega, t)$  [20]:

$$= \frac{-1}{\pi} Im \left( \sum_{m,n} \frac{\langle \Psi(t) | c_j^\dagger | \Psi_n \rangle \langle \Psi_n | c_j | \Psi_m \rangle \langle \Psi_m | \Psi(t) \rangle}{e_n - e_m + \omega + i\eta} \right). \quad (6)$$

Similarly, the hole component of  $LD_j(\omega, t)$  at site  $j$  can be written as  $LD_j^h(\omega, t)$  [20]:

$$= \frac{-1}{\pi} Im \left( \sum_{m,n} \frac{\langle \Psi(t) | \Psi_n \rangle \langle \Psi_n | c_j | \Psi_m \rangle \langle \Psi_m | c_j^\dagger | \Psi(t) \rangle}{e_n - e_m + \omega + i\eta} \right). \quad (7)$$

Interestingly, with increase in the couplings  $t_h(t)$  and  $\Delta(t)$ , the electron  $LD_j^e(\omega, t)$  and hole  $LD_j^h(\omega, t)$  both shows

equal-height sub-gap peaks close to  $\omega = \pm t_h(T) \frac{2t}{\tau}$  (in the rest of the paper, we use  $t_h(T) = 1$ ) for  $V = 0.05$ , reflecting the formation of equal amounts of electron and hole at positive and negative values of  $\omega$  [see Figs. 2(g,h,i)]. This is in contrast to the static case, where only an electron forms at negative values of  $\omega$  and only a hole forms at positive values of  $\omega$  [ Figs. 2(d,e,f)]. Thus, the appearance of equal magnitude electron and hole components at both frequencies  $\omega = \pm 2t/\tau$ , is clearly a non-equilibrium effect and it is influenced by the conservation of total parity of  $|\Psi(t)\rangle$ . Due to this dynamics, the time-evolving wavefunction  $|\Psi(t)\rangle$  has an equal overlap with low-energy states  $|\Psi_1\rangle$  and  $|\Psi_3\rangle$  (with same total parity  $P = +1$ ). This allows for similar spectral weights close to  $\omega = -2t/\tau$  in  $LD_j^e(\omega, t)$  (transition from state  $m = 1$  to  $n = 4$ ) and  $LD_j^h(\omega, t)$  (from state  $m = 2$  to  $n = 3$ ), and also similar spectral weights close to  $\omega = +2t/\tau$  in  $LD_j^e(\omega, t)$  (resulting from a transition from state  $m = 3$  to  $n = 2$ ) and in  $LD_j^h(\omega, t)$  (from state  $m = 4$  to  $n = 1$ ).

The equal superposition of two low-energy many-body states in  $|\Psi(t)\rangle$  even for large  $\tau = 100$  (we have also checked for the case  $\tau = 500$  and the results are the same) is a unique property of non-trivial fusion. In the trivial fusion for the larger  $\tau$ , the time evolving wave-function  $|\Psi(t)\rangle$  overlap only with one low-energy state of the instantaneous ground states manifold of the time evolving Hamiltonian. Introducing a time-dependent hopping  $t_h(t)$  and pairing  $\Delta(t)$ , the fuse of the MZMs  $\gamma_2$  and  $\gamma_3$  occurs non-trivially because the MZMs are from different pairs. The  $t_h(t)$  and  $\Delta(t)$  allows for tunneling of a single electron (or a pair of electrons) from the left to the right chain portions during the fusion process, which changes the individual parities of those left and right quantum-dot segments, but the total parity of the many-body state  $|\Psi(t)\rangle$  remains the same [30]. This results in the formation of both fermion  $\Psi$  and vacuum  $I$  channels, after fusion of  $\gamma_2$  and  $\gamma_3$  non-trivially (see [31] for more details). At the final time  $t = T$ , the system has two MZMs ( $\gamma_1$  and  $\gamma_4$ ) at the left and right edge of the chain (see Fig. 2b).

Now increasing the repulsive Coulomb interaction  $V$  leads to asymmetrical spectral weight at  $\omega = \pm 2t/\tau$  as time increases [see Figs. 2(j,k,l)]. For larger value of  $V$ , the cost of adding an electron at site  $j = 6$  (or  $j = 7$ ) for state  $|\Psi_2\rangle$  is costlier than adding an electron to state  $|\Psi_4\rangle$  (see also the electron density for low-energy states in the SM). This results in larger spectral weight at  $\omega = -2t/\tau$  compared to  $\omega = +2t/\tau$  in the electron and hole parts of the local-density of states  $LD_j(\omega, t)$ .

In summary, we have found an equal spectral weight for electron and hole components in the time-dependent local density of states during the non-trivial fusion process of Majoranas form different pairs. Interestingly the time-evolving state becomes an almost equal-linear superposition of two low-energy states, even for larger values of  $\tau$ . The formation of a similar magnitude of electron and hole confirms the non-trivial nature of Majorana fermions. The increase in Coulomb interaction leads to asymmetry in the peaks close to  $\omega = \pm 2t/\tau$ .

**(b) The case  $\phi_1 = \pi$ , and  $\phi_2 = 0$**

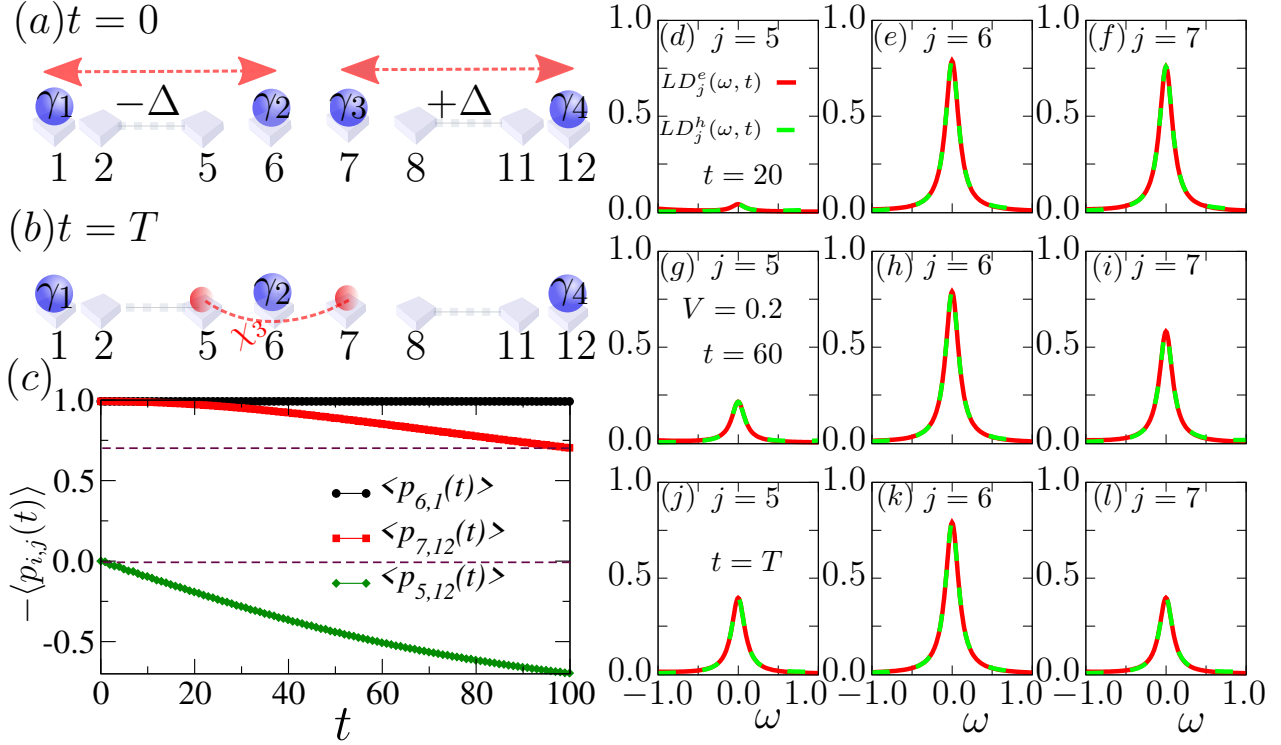


FIG. 3. (a) Schematic representation of two pairs of MZMs [ $(\gamma_1, \gamma_2)$  and  $(\gamma_3, \gamma_4)$ ]: at time  $t = 0$  the left part has pairing coupling strength  $-\Delta$ , while the right part has pairing coupling strength  $+\Delta$ . (b) Pictorial representation for the formation of a multi-site MZM ( $\chi_3$ ) at time  $t = T$ . (c) Time-dependent parity  $-\langle P_{i,j}(t) \rangle$  as a function of time  $t$  for different pairs of Majoranas and at  $V = 0.1$ . The electron and hole components of the time-dependent local density of state  $LD_j^e(t)$  and  $LD_j^h(t)$  at time  $t = 20$  and for sites: (d)  $j = 5$ , (e)  $j = 6$ , and (f)  $j = 7$ . The  $LD_j^e(t)$  and  $LD_j^h(t)$  at intermediate time  $t = 60$  and for sites: (g)  $j = 5$ , (h)  $j = 6$ , and (i)  $j = 7$ . The  $LD_j^e(t)$  and  $LD_j^h(t)$  at the final time  $t = T$  and for sites: (j)  $j = 5$ , (k)  $j = 6$ , and (l)  $j = 7$ .

In this sub-section, we will study the Majorana fusion in a  $\pi$ -junction setup. In order to form a  $\pi$ -junction between the right and left quantum-dot arrays, we consider two pairs of MZMs, in this case with opposite signs of the pairing terms ( $-\Delta$  for the left array, and  $+\Delta$  for the right array). The MZMs in the left quantum-dots array has definite parity  $P_{6,1} = -i\langle \gamma_6 \gamma_1 \rangle = -1$  and the right pair has definite parity  $P_{7,12} = -i\langle \gamma_7 \gamma_{12} \rangle = -1$  as well (see Fig. 3a). At  $t = 0$  there are no hopping and pairing terms between the left and right arrays.

Next, we turn on the time-dependent hopping ( $t_h$ ) and pairing  $\Delta(t)$  terms (with zero phase factor as example) between the left and right arrays, which effectively makes a time-dependent  $\pi$ -junction quantum-dot array. In order to observe the behavior of the central Majoranas  $\gamma_2$  and  $\gamma_3$ , we calculate the time-dependent electron  $LD_j^e(t)$  and hole  $LD_j^h(t)$  portions of the local-density of state for sites  $j = 5, 6$  and  $7$ . At  $t = 0$  the electron  $LD_j^e(t)$  and hole  $LD_j^h(t)$  portions of the local-density of states shows equal height peaks at  $\omega = 0$  for the sites  $j = 6$  and  $7$ , which indicate the presence of two localized MZMs.

For the time  $t = 20$ , the  $LD_j^e(t)$  and  $LD_j^h(t)$  [see Figs. 3(d,e,f)] shows small peaks at  $\omega = 0$  for site  $j = 5$ , and larger peaks for sites  $j = 6$  and  $j = 7$  at  $\omega = 0$ . Increasing

time to  $t = 60$  [ Figs. 3(g,h,i)] the peak height of  $LD_j^e(t)$  and  $LD_j^h(t)$  increase for site  $j = 5$ , remain *constant* for site  $j = 6$ , and decrease for site  $j = 7$ . This spectral weight shift suggests the *tunneling* of MZM  $\Gamma_3$  from site  $j = 7$  to  $j = 5$ . Note that the height of peaks at  $\omega = 0$ , for the electron  $LD_j^e(t)$  and hole  $LD_j^h(t)$  parts of the local-density of states are almost equal for each site for all times  $t$ . We also find that the spectral weight at  $\omega = 0$ , mainly arises from the low-energy sub-space of four-fold degenerate states. The equal-contribution of electron and hole part of the local-density of states at  $\omega = 0$  for these central sites, shows the presence of Majorana zero modes at sites  $j = 5, 6$ , and  $7$ .

At the final time  $t = T = 100$ , the  $LD_j^e(t)$  and  $LD_j^h(t)$  have almost equal height peaks for sites  $j = 5$  and  $j = 7$  and the total spectral weights on these two sites is close to localized on-site MZM, confirming the formation of the multi-site MZM  $\chi_3$  (see Fig. 3b). The  $LD_j^e(t)$  and  $LD_j^h(t)$  for site  $j = 6$  remain constant all up to time  $t = T$ . Thus, the transfer of spectral weight from site  $j = 7$  to  $j = 5$  at  $\omega = 0$ , hints to a tunneling effect of half of the MZM  $\gamma_3$  from site  $j = 7$  to site  $j = 5$ , leading to formation of a multi-site MZM  $\chi_3$ . This is a novel effect not reported before.

Interestingly, the low-energy four states remains

degenerate, even after switching the time-dependent hopping  $t_h(t)$  and pairing  $\Delta(t)$  terms between the left and right arrays, showing the presence of a total of four MZMs in the system. We also find that the time-evolving wavefunction  $|\Psi(t)\rangle = u|\Psi_1\rangle + v|\Psi_4\rangle$  becomes a superposition of two low-energy degenerate ground states (with the same total parity). The amplitudes  $u$  and  $v$  depend on the tunneling of the MZM  $\gamma_3$  from site  $j = 7$  to site  $j = 5$  (for  $t = 20$   $|u|^2 = 0.8$  and  $|v|^2 = 0.2$ ). These amplitudes  $u$  and  $v$  remain the same for different values of large  $\tau$ . Furthermore, to confirm the tunneling of MZM  $\gamma_3$ , we also calculate the time-dependent parity  $\langle P_{ij}(t) \rangle = -\langle \Psi(t) | \gamma_i \gamma_j | \Psi(t) \rangle$ , for different pairs of Majoranas. As shown in Fig. 3c, the observable  $\langle p_{6,1}(t) \rangle$  remains constant with time, showing that the MZM  $\gamma_2$  remains localized at site  $j = 6$ , without any change in parity of the pair  $(\gamma_1, \gamma_2)$ . Meanwhile,  $\langle p_{7,12}(t) \rangle$  starts decreasing and approach the value  $1/\sqrt{2}$ , at time  $t = T$ . On the other hand,  $\langle p_{5,12}(t) \rangle$  becomes non-zero as time increases and approaches  $-1/\sqrt{2}$ . Once again, these results suggest the formation of a multi-site MZM with form  $\chi_3 = -\frac{1}{\sqrt{2}}\gamma_5 + \frac{1}{\sqrt{2}}\gamma_7$ , where one component of  $\chi_3$  appears due to tunneling of  $\gamma_3$  initially localized on site  $j = 7$ .

For the ground-state one-dimensional Kitaev-wire with  $\pi$ -junction, there are a total of four MZMs. To understand the behavior of the central MZMs, using just three central sites ( $j = 5, 6$ , and  $7$ ), we can write the Hamiltonian for the central region as (with  $\phi_1 = \pi$  and  $\phi_2 = 0$  for the two central bonds respectively):

$$H^{III} = -2i\Delta \left( \gamma_5^B \gamma_6^B + \gamma_7^A \gamma_6^B \right), \quad (8)$$

where we used the relations  $c_5 = \frac{1}{\sqrt{2}}e^{-i\phi_1/2} \left( \gamma_5^A + i\gamma_5^B \right)$ ,  $c_6 = \frac{1}{\sqrt{2}} \left( \gamma_6^A + i\gamma_6^B \right)$ ,  $c_7 = \frac{1}{\sqrt{2}}e^{-i\phi_2/2} \left( \gamma_7^A + i\gamma_7^B \right)$ . Interestingly, the Majorana operator  $\gamma_6^A$  is absent in the Hamiltonian, showing that  $\gamma_6^A$  is a single-site MZM mode at site 6. The form of the Hamiltonian also suggests that one localized mode,  $\gamma_6^A$ , does not interact with any other Majorana zero mode, which could be the reason of localization of the initial Majorana mode located at site  $j = 6$ . After diagonalizing the Hamiltonian  $H^{III}$ , we find that a multi-site MZM  $\chi_3 = -\frac{1}{\sqrt{2}}\gamma_5 + \frac{1}{\sqrt{2}}\gamma_7$  resides at sites  $j = 5$  and  $j = 7$  (see the SM of Ref [19] for a more detail calculation). This ground state results indicate that out of an initial total of four single-site MZMs, there are now three single-site local MZMs (two localized at edge end sites and one at central site  $j$ ) and one multi-site MZM with form  $\chi_3 = -\frac{1}{\sqrt{2}}\gamma_j + \frac{1}{\sqrt{2}}\gamma_{j+2}$ .

In summary, the Majoranas near the  $\pi$ -junction do not fuse. Instead, one MZM remains a localized single-site MZM, and another transforms into a multi-site MZM (located on two sites with equal amplitude). The tunneling of half of the second MZM through the centrally localized one-site MZM in a strict one-dimensional geometry is interesting and certainly a novel effect. This partial tunneling of a Majorana leads to the time-evolving wavefunction in a superposition of two low-energy degenerate states (with same total parity).

## Non-trivial fusion of MZMs in Y-shape quantum dot arrays

This section will study the fusion of three MZMs from different pairs, further increasing the complexity of the problem. The presence of multiple Majoranas can occur in topological materials or in quantum circuits experiments. The overlap between odd and even numbers of Majoranas can give different behavior in the tunneling spectra [32]. Here, we simulate the overlap between an odd number (three) of MZMs as a function of time, starting with fully separated MZMs. We consider a Y-shape geometry consisting of three quantum-dot chains at the sweet spot and with the same superconducting phase  $\phi_1 = \phi_2 = \phi_3 = 0$  at each arm. At time  $t = 0$ , there is no hopping and superconducting coupling between these three quantum-dot arrays. As shown in Fig. 4a, the system has three pairs of Majorana zero modes  $(\gamma_1, \gamma_2)$ ,  $(\gamma_3, \gamma_4)$ , and  $(\gamma_5, \gamma_6)$ , with well-defined initial parities  $P_{12} = -i\langle \gamma_1 \gamma_2 \rangle = +1$ ,  $P_{34} = -i\langle \gamma_3 \gamma_4 \rangle = +1$ , and  $P_{56} = -i\langle \gamma_5 \gamma_6 \rangle = +1$ . The six Majorana modes at the sweet-spot ( $t_h = \Delta = 1$  and  $V = 0$ ) give rise to an eight-fold degenerate ground state, because we can form three non-local spinless fermions (which give rise to  $2^3 = 8$  fold degeneracy). Within an eight-fold degenerate ground state, four states have individual total parity  $P = +1$  and the remaining four have parity  $P = -1$ . Using the four-degenerate ground state with fixed same parity one can encode two topological qubits, which can display all the basic operations for topological quantum computation [33].

The Hamiltonian for the Y-shaped quantum-dot array (with  $\phi_1 = \phi_2 = \phi_3 = 0$  at each arm) can be divided into four different parts. The Hamiltonian for each arm can be written as:

$$H^I = \sum_{j=1}^{l-1} \left( -t_h c_j^\dagger c_{j+1} + \Delta c_j c_{j+1} + H.c. \right), \quad (9)$$

$$H^{II} = \sum_{j=l+1}^{2l-1} \left( -t_h c_j^\dagger c_{j+1} + \Delta c_j c_{j+1} + H.c. \right), \quad (10)$$

$$H^{III} = \sum_{j=2l+1}^{3l-1} \left( -t_h c_j^\dagger c_{j+1} + \Delta c_j c_{j+1} + H.c. \right). \quad (11)$$

Moreover, in order to fuse the MZMs from different pairs, first we switch on the time-dependent pairing  $\Delta(t)$  and hopping  $t_h(t)$  terms between each arm. In practice, we tune the time-dependent pairing and hopping terms as  $\Delta(t) = t_h(t) = t_h(T) \frac{n\delta t}{\tau}$  between the central three MZMs  $(\gamma_2, \gamma_3, \gamma_5)$ . We used  $\tau = 100$  and other parameters as described in the previous cases.  $T$  is the final time such that  $\Delta(t) = t_h(t) = 1$  at  $t = T = 100$ . The time-dependent Hamiltonian coupling the arm edges is written as:

$$\begin{aligned} H^C(t) = & -t_h(t) c_l^\dagger c_{l+1} + \Delta(t) c_l c_{l+1} + H.c. \\ & -t_h(t) c_{l+1}^\dagger c_{2l+1} + \Delta(t) c_{l+1} c_{2l+1} + H.c. \\ & -t_h(t) c_l^\dagger c_{2l+1} + \Delta(t) c_l c_{2l+1} + H.c. \end{aligned} \quad (12)$$

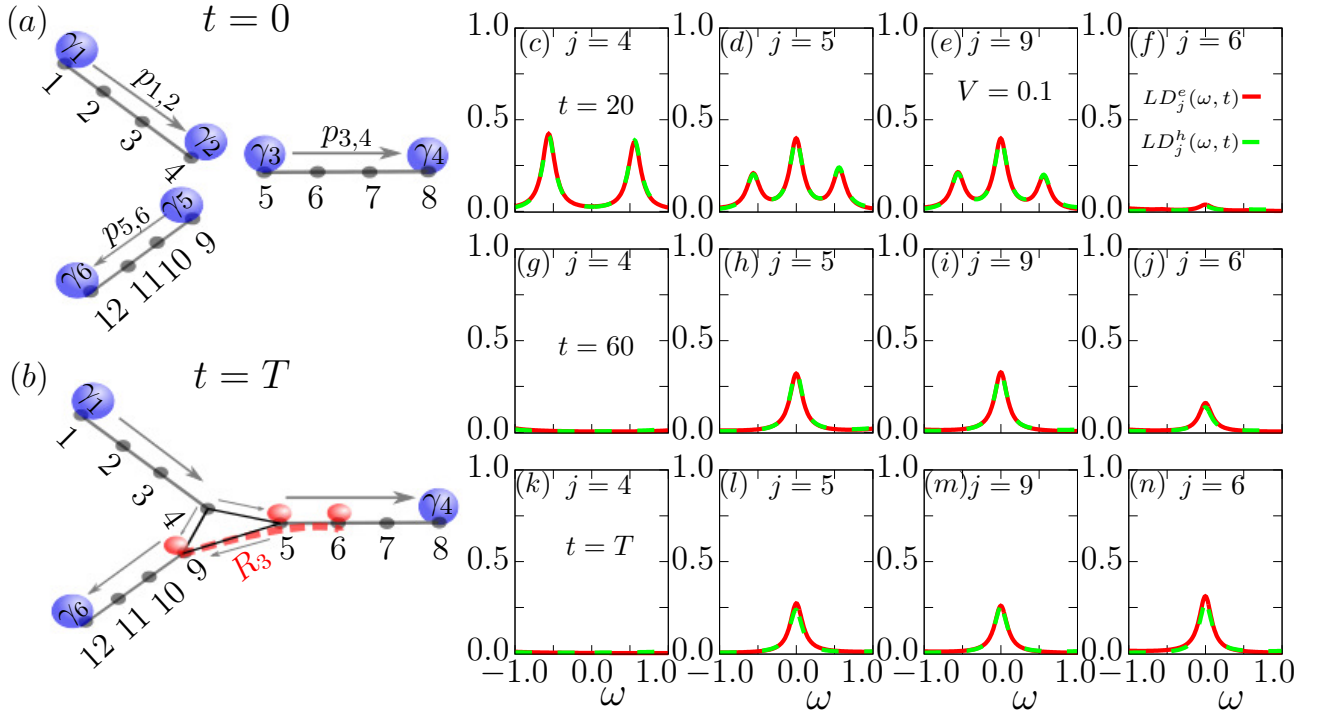


FIG. 4. (a) Schematic representation of three pairs of Majorana zero modes in a Y-shape Kitaev wire. At  $t = 0$ , each pair has fixed fermionic parity  $P_{1,2} = +1$ ,  $P_{3,4} = +1$ , and  $P_{5,6} = +1$ . The direction of the arrows denote the directions of the pairing terms  $\Delta$  and site index  $j$  in each wire. (b) Pictorial representation of the formation of the multi-site MZM  $R_3$  after the fusion of the three central MZMs at time  $t = T$ , after the adiabatic process ends. The time-dependent electron  $LD_j^e(\omega, t)$  and hole  $LD_j^h(\omega, t)$  portions of the local-density of states at time  $t = 20$  and for sites (c)  $j = 4$ , (d)  $j = 5$ , (e)  $j = 9$ , and (f)  $j = 6$ . The  $LD_j^e(\omega, t)$  and  $LD_j^h(\omega, t)$  for the intermediate time  $t = 60$  and for sites (g)  $j = 4$ , (h)  $j = 5$ , (i)  $j = 9$ , and (j)  $j = 6$ . The  $LD_j^e(\omega, t)$  and  $LD_j^h(\omega, t)$  for the final time  $t = T$  and for sites (k)  $j = 4$ , (l)  $j = 5$ , (m)  $j = 9$ , and (n)  $j = 6$ . These numerical calculations were performed using  $L = 12$  sites and  $t_h = \Delta = 1$ ,  $V = 0.1$ .

Using the above Hamiltonian  $H = H^I + H^{II} + H^{III} + H^C(t)$ , we performed the time evolution starting from the ground state with total parity  $P = +1$ , and calculated the electron  $LD_j^e(\omega, t)$  and hole  $LD_j^h(\omega, t)$  portions of the local-density of states for various times  $t$ . At  $t = 0$ , we find that the central edge sites  $j = 4, 5$ , and  $9$  in  $LD_j^e(\omega, t)$  and  $LD_j^h(\omega, t)$  have sharp peaks at  $\omega = 0$ . Introducing a time-dependent hopping and pairing term leads to the simultaneous fusion of three central MZMs ( $\gamma_2, \gamma_3, \gamma_5$ ), the three belonging to different original MZM pairs. The fusion of central MZMs leads to a split in the initial eight-fold degenerate ground state into two sets of low-energy four-fold degenerate states.

As shown in Fig. 4c, the time-dependent electron  $LD_j^e(\omega, t)$  and hole  $LD_j^h(\omega, t)$  portions of the local-density of states at time  $t = 20$ , for site  $j = 4$ , shows peaks close to  $\omega = \pm \frac{3t}{\tau}$ , indicating the formation of both electron and hole for positive and negative frequencies. Using Eqs. 6 and 7, we find the spectral weights at  $\omega = \pm \frac{3t}{\tau}$  in the electron and hole parts of  $LD_j(\omega, t)$  arise from the transition between the splitted two-set of four-fold degenerate states [mainly ( $n = 2$  to  $m = 6$ ) or ( $n = 1$  to  $m = 5$ )]. In fact, the time-evolving state  $|\Psi(t)\rangle$  becomes a superposition of four states (two from the lower four-fold degenerate part and rest two from the

other four-fold states of the eight-fold low-energy states) of the instantaneous Hamiltonian.

At sites  $j = 5$  and  $9$  [ Figs. 4(d,e)], the  $LD_j^e(\omega, t)$  and  $LD_j^h(\omega, t)$ , shows peaks at  $\omega = 0$  and also close to  $\omega = \pm \frac{3t}{\tau}$ , with equal spectral weight of the electron and hole portions of the time-dependent local-density of states. These results for the sites  $j = 5$  and  $9$  show that the MZMs still survive for these sites and in addition there is a formation of electron and hole close to  $\omega = \pm \frac{3t}{\tau}$  due to the partial fusion of MZMs. Interestingly, for site  $j = 6$ , a small peak appears at  $\omega = 0$ .

For the intermediate time  $t = 60$ , the  $LD_j^e(\omega, t)$  and  $LD_j^h(\omega, t)$  in the range of  $-1 \leq \omega \leq 1$ , there is no peak for site  $j = 4$ . On the other hand, for sites  $j = 5$  and  $9$  the peaks at  $\omega = 0$  decreases with time and for site  $j = 6$  shows a peak at  $\omega = 0$  and the peak strength increases with increasing time  $t$ . These results show the *transfer* of spectral weight from the central sites ( $j = 5$  and  $9$ ) to the site  $j = 6$ . For the final time after the adiabatic process,  $t = T$ , the  $LD_j^e(\omega, t)$  and  $LD_j^h(\omega, t)$  show almost equal-height peaks at  $\omega = 0$  for the three central sites  $j = 5, 9$  and  $6$ , see Figs. 4(l,m,n). These results indicate the formation of equal amount of electron and hole, and, surprisingly, just one multi-site MZM after the fusion of three central MZMs ( Fig. 4b). In other words, we unveiled the unexpected and novel result that the fusion of

three one-site MZMs leads to a single MZM spread on three sites.

In summary, in comparison to the fusion of two MZMs (even numbers), the fusion of three MZMs (odd numbers) give rise to a novel multi-site MZM. The local density of states shows peaks at  $\omega = 0$  for three different central sites. Note that the multi-site MZM position depend on the pairing terms' direction. The appearance of a multi-site MZM near the central part is mainly due to the different coupling directions (effectively a  $\pi$ -junction) at the tri-junction (see Fig. 4b).

## Discussion

In this publication, we studied the non-trivial fusion of Majorana zero modes in canonical chains, as well as in a Y-shape array of interacting quantum dots close to the sweet spot in parameter space. We examined the real-time dynamics of the local density-of-states to reveal the nature of the non-trivial fusion of MZMs. The Majoranas were initialized in pairs with definite parity in separate quantum-dot arrays. Varying the time-dependent hopping and pairing terms between the different quantum-dot arrays, we carry out the fusion of Majoranas from different pairs (non-trivial fusion). We observed the fusion outcomes by calculating the time-dependent electron and hole part of the local-density of states. Several unexpected results were unveiled:

(1) In the case of a one-dimensional chain with the same phase on each left and right wire, we demonstrated the formation of both electron and hole close to  $\omega = \pm 2t/\tau$  in equal magnitude for small values of Coulomb interactions. The formation of equal amount of electron and hole at each  $\omega = \pm 2t/\tau$  value is a dynamical effect and reveals the non-trivial nature of the MZMs fusion. In fact, we find that the time-evolving states becomes an equal superposition of two states (with the same parities). This non-equilibrium effect is unique in case of the non-trivial fusion. For the trivial fusion the time-evolving states overlaps with only one state of the instantaneous Hamiltonian. For the first time, we explore the effect of Coulomb interaction on the dynamics of non-trivial fusion. The Coulomb interaction leads to asymmetry in the peak height at  $\omega = \pm 2t/\tau$ , as adding an electron is costlier to the low-energy state. Although it is gratifying to observe these effects in actual many-body calculations, the equal mixture of electron and hole in the outcome was intuitively expected.

(2) On the other hand, quite unexpected results were found for the case of a  $\pi$ -junction (with opposite phase on each left and right wire) because the Majoranas do not fuse with one another. Instead they formed a multi-site MZM residing on two sites near to an independent localized one-site central MZM. The time-average parity and time-dependent local-density of states reveals that the one-site MZM at the edge (near the center) of the left array does not fuse with other MZMs and remain localized on the same edge site. Surprisingly, half the MZM of the right quantum-dot array (near the center) *tunnels* through the localized one-site MZM and forms a multi-site MZM. The tunneling of half of the MZM even in a strict one-dimensional geometry is a quite novel effect. The tunneling of MZM also makes

the time-evolving state become a superposition of two states from the four-fold degenerate ground state manifold of the instantaneous Hamiltonian even for smaller quench rate. The amplitude of the two states in the time-evolving state depends on the amount of tunnel MZM through the central localized MZM.

(3) For the fusion of MZMs in a Y-shape quantum-dot array, where the MZMs are coupled through time-dependent hopping and pairing terms in a triangular geometry, we show the formation of an exotic multi-site MZM after the fusion of three central MZMs from different pairs. Interestingly, the time-evolving state becomes a superposition of four states of instantaneous Hamiltonian (two from the lower four-fold degenerate and other two form higher four-fold degenerate states), due to the non-trivial fusion and formation of multi-site MZM. In general terms, the nature and behavior of the central multi-sites MZMs are dependent on the geometry and direction of the pairing terms of quantum-dot arrays. The knowledge of the characteristics of the central multi-sites MZMs is important for the braiding of MZMs in dynamical and realistic settings, where the exchange of MZMs is performed by moving the MZMs adiabatically. In comparison to the previously studied MZM fusion in the non-interacting single particle picture, here we do not find any density fluctuations during the non-trivial fusion of MZMs (in one-dimensional geometry), using the time-evolving many-body wave-function. The formation of electron and hole clearly appears in the electron and hole parts of the time-dependent local-density of states. The local-density of states can be measured in tunneling-spectroscopy in quantum-dot experiments.

The study of non-trivial fusion is related to the non-Abelian statistics and can be performed in the present quantum-dot setups. The observation of fusion outcome should be more accessible than performing braiding experiments. We believe our novel findings of the non-trivial fusion of Majoranas in the one-dimensional chain and Y-shape geometries can be realized using the recently developed quantum-dot setups. Our prediction of the fusion outcome, based on the time-dependent local density-of-state method, is accessible to the present-day experimental capability [6].

## Methods

In order to calculate the time-dependent local density-of-states, we use the exact-diagonalization method [20]. First, we time evolve the initial wave function  $|\Psi(0)\rangle$  up to time  $t$ , using the time-dependent Hamiltonian  $H(t)$  as:  $|\Psi(t)\rangle = \mathcal{T} \exp\left(-i \int_0^t H(s) ds\right) |\Psi(0)\rangle$ , where  $\mathcal{T}$  is the time ordering operator [34]. Next, we calculate the double-time Green function  $G(t, t')$  [35], using the instantaneous Hamiltonian  $H_f = H(t = t_f)$  at time  $t = t_f$ :

$$G_j^{elec}(t, t') = \langle \Psi(t) | c_j^\dagger e^{iH_f t'} c_j e^{-iH_f t} | \Psi(t) \rangle. \quad (13)$$

The time-dependent  $LD_j^e(\omega, t)$  for the electronic part of the local-density of state is the Fourier transform of the local



Green function at site  $j$  with respect to  $t'$ :

$$LD_j^e(\omega, t) = \frac{1}{\pi} \text{Im} \int_0^T dt' e^{i(\omega+i\eta)t'} iG_j^{elec}(t, t'), \quad (14)$$

where we use  $T = 60$  for the integration. The broadening parameter was fixed to  $\eta = 0.1$  in the entire publication. Similarly, the hole part  $LD_j^h(\omega, t)$  of the local density-of-states has been calculated using the Fourier transform of the Green function  $G_j^{hole}(t, t') = \langle \Psi(t) | c_j(t') c_j^\dagger | \Psi(t) \rangle$ . The total local density-of-states at site  $j$  can be written as  $LD_j(\omega, t) = LD_j^h(\omega, t) + LD_j^e(\omega, t)$  [20].

#### Data availability

The data that support the findings of this study are available from the corresponding author upon request.

#### Code availability

The computer codes used in this study are available from the corresponding author upon request.

#### Acknowledgments

The work of B.P., S.O., and E.D. was supported by the U.S. Department of Energy (DOE), Office of Science, Basic Energy Sciences (BES), Materials Sciences and Engineering Division.

#### Author contributions

B.P. and E.D. designed the project. B.P. carried out the calculations for the Y-shaped Kitaev model. B.P., S.O., and E.D. wrote the manuscript. All co-authors provided useful comments and discussion on the paper.

#### Competing interests

The authors declare no competing interests.

#### Additional information

Correspondence should be addressed to Bradraj Pandey ([bradraj.pandey@gmail.com](mailto:bradraj.pandey@gmail.com)).

- 
- [1] Kitaev AY. Fault-tolerant quantum computation by anyons. *Ann Phys (NY)* **303**, 2 (2003).
- [2] Sarma, S., Freedman, M. Nayak, C. Majorana zero modes and topological quantum computation. *npj Quantum Inf* **1**, 15001 (2015).
- [3] Nayak C, Simon SH, Stern A, Freedman M, Sarma SD. Non-abelian anyons and topological quantum computation. *Rev Mod Phys* **80**, 1083 (2008).
- [4] Kitaev AY. Unpaired Majorana fermions in quantum wires. *Phys.-Usp.* **44**, 131 (2001).
- [5] Scheurer, M. S., & Shnirman. Nonadiabatic processes in Majorana qubit systems. *Phys. Rev. B* **88**, 064515 (2013).
- [6] Dvir, T., Wang, G., van Loo, N. et al. Realization of a minimal Kitaev chain in coupled quantum dots. *Nature* **614**, 445450 (2023).
- [7] Sau, J., Sarma, S. Realizing a robust practical Majorana chain in a quantum-dot-superconductor linear array. *Nat Commun.* **3**, 964 (2012).
- [8] Tsintzis, A., Souto, R. S., Leijnse, M. Creating and detecting poor man's Majorana bound states in interacting quantum dots. *Phys. Rev. B* **106**, L201404 (2022).
- [9] Mills, A.R., Zajac, D.M., Gullans, M.J. et al. Shuttling a single charge across a one-dimensional array of silicon quantum dots. *Nat Commun.* **10**, 1063 (2019).
- [10] Deng, M. T., Vaitiekėnas, E., Hansen, E. B., Danon, J. et al. Majorana bound state in a coupled quantum-dot hybrid-nanowire system. *Science* **354**, 15571562 (2016).
- [11] Rančić, J. M., Hoffman, S., Schrade, C., Klinovaja, J., & Loss, D. Entangling spins in double quantum dots and Majorana bound states. *Phys. Rev. B* **99**, 165306 (2019)
- [12] Wang, G. et al Singlet and triplet Cooper pair splitting in superconducting-semiconducting hybrid nanowires. *Nature* **612**, 448 (2022).
- [13] Wang, Q. ten Haaf, S.L.D., Kulesh, I. et al. Triplet correlations in Cooper pair splitters realized in a two-dimensional electron gas. *Nat Commun.* **14** 4876 (2023).
- [14] Liu, C.-X., Wang, G., Dvir, T. & Wimmer, M. Tunable superconducting coupling of quantum dots via Andreev bound states in semiconductor-superconductor nanowires. *Phys. Rev. Lett.* **129**, 267701 (2022)
- [15] Pan, H. & Sarma, S. D. Disorder effects on Majorana zero modes: Kitaev chain versus semiconductor nanowire. *Phys. Rev. B* **103**, 224505 (2021).
- [16] Aasen, D., Hell, M., Mishmash, R. V., Higginbotham, A., et al. Milestones toward Majorana-based quantum computing. *Phys. Rev. X* **6**, 031016 (2016).
- [17] Alicea, J., Oreg, Y., Refael, G. et al. Non-Abelian statistics and topological quantum information processing in 1D wire networks. *Nature Phys.* **7**, 412417 (2011).
- [18] Leijnse, M. & Flensberg, K. Parity qubits and poor man's Majorana bound states in double quantum dots. *Phys. Rev. B* **86**, 134528 (2012).
- [19] Pandey, B., Kaushal, N., Alvarez, G. et al. Majorana zero modes in Y-shape interacting Kitaev wires *npj Quantum Mater.* **8** 51 (2023).
- [20] Pandey, B., Mohanta, N., Dagotto, E. Out-of-equilibrium Majorana zero modes in interacting Kitaev chains. *Phys. Rev. B* **107**, L060304 (2023).
- [21] Zhou, T., Dartiailh, M.C., Sardashti, K., Han, J. E. et al. Fusion of Majorana bound states with mini-gate control in two-dimensional systems. *Nat Commun.* **13**, 1738 (2022).
- [22] Bai, J., Wang, Q., Xu, L., Feng, W. & Li, X. *arXiv:2309.13566*. (2023).
- [23] Liu, C., Pan, H. Setiawan, F. et al. Fusion protocol for Majorana modes in coupled quantum dots. *Phys. Rev. B* **108**, 085437 (2023).
- [24] Zhang, H., Liu, D.E., Wimmer, M. et al. Next steps of quantum transport in Majorana nanowire devices. *Nat Commun.* **10**, 5128 (2019).
- [25] Bordin, A., Li, X., Driel, D. V., Wolff, J. C. et al. Crossed Andreev reflection and elastic co-tunneling in a three-site Kitaev chain nanowire device. *arXiv: 2306*, 07696 (2023).
- [26] Michiel W A de Moor et al. Electric field tunable superconductor-semiconductor coupling in Majorana

- nanowires. *New J. Phys.* **20**, 103049 (2018).
- [27] Chiu, C. Vazifeh, M. M., & Franz, M. Majorana fermion exchange in strictly one-dimensional structures. *EPL* **110**, 10001 (2015).
- [28] Turner, A. M., Pollmann, F., & Berg, E. Topological phases of one-dimensional fermions: An entanglement point of view. *Phys. Rev. B* **83**, 075102 (2011).
- [29] Herbrych, J., Środa, M., Alvarez, G., Dagotto, E. Interaction-induced topological phase transition and Majorana edge states in low-dimensional orbital-selective Mott insulators. *Nat Commun.* **12**, 2955 (2021).
- [30] Karki, D. B., Matveev, K. A., & Martin, I. Physics of the Majorana-superconducting qubit hybrids. *arXiv*: **2309**, 08758 (2023).
- [31] See the Supplemental Material for the detailed analytical calculations.
- [32] Flensberg, K. Tunneling characteristics of a chain of Majorana bound states. *Phys. Rev. B* **82**, 180516(R) (2010).
- [33] Lahtinen, V. T. & Pachos, J. K. A Short Introduction to Topological Quantum Computation. *SciPost Phys.* **3**, 021 (2017).
- [34] Kells, G. et al. Topological blocking in quantum quench dynamics. *Phys. Rev. B* **89**, 235130 (2014).
- [35] Kennes, D. M., Klöckner, C., & Meden, V. Spectral Properties of One-Dimensional Fermi Systems after an Interaction Quench. *Phys. Rev. Lett.* **113**, 116401 (2014).